IEEE Photonics Journal
An IEEE Photonics Society Publication

Open Access

Measuring Hanbury Brown and Twiss Effect of Multi-Spatial-Mode Thermal Light at Ultrashort Timescale by Two-Photon Absorption

Volume 10, Number 6, December 2018

Zhiguo Tang
Bin Bai
Yu Zhou
Huaibin Zheng
Hui Chen
Jianbin Liu
Fuli Li
Zhuo Xu

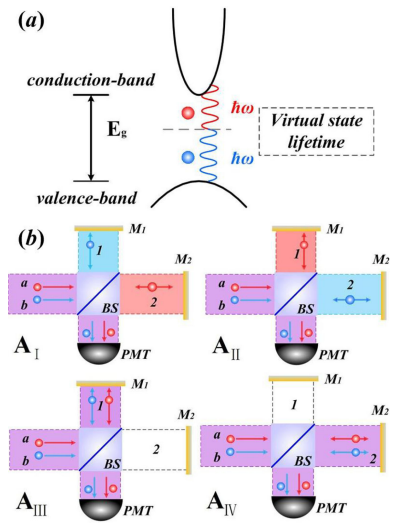

DOI: 10.1109/JPHOT.2018.2879973
1943-0655 © 2018 IEEE

Measuring Hanbury Brown and Twiss Effect of Multi-Spatial-Mode Thermal Light at Ultrashort Timescale by Two-Photon Absorption

Zhiguo Tang,[1] Bin Bai,[1,2] Yu Zhou,[3] Huaibin Zheng,[1] Hui Chen,[1] Jianbin Liu,[1] Fuli Li,[3] and Zhuo Xu[1]

[1]Electronic Materials Research Laboratory, Key Laboratory of the Ministry of Education and International Center for Dielectric Research, School of Electronic and Information Engineering, Xi'an Jiaotong University, Xi'an 710049, China
[2]Beijing Institute of Remote Sensing Information, Beijing 100192, China
[3]MOE Key Laboratory for Nonequilibrium Synthesis and Modulation of Condensed Matter, Department of Applied Physics, Xi'an Jiaotong University, Xi'an 710049, China

DOI:10.1109/JPHOT.2018.2879973

Manuscript received July 2, 2018; revised October 23, 2008; accepted November 2, 2018. Date of publication November 7, 2018; date of current version November 20, 2018. This work was supported in part by the National Basic Research Program of China (973 Program) under Grant 2015CB654602, in part by the 111 Project of China under Grant B14040, in part by the Fundamental Research Funds for the Central Universities. Corresponding author: Huaibin Zheng (e-mail: huaibinzheng@xjtu.edu.cn).

Abstract: Hanbury Brown and Twiss effect of multi-spatial-mode thermal light is obtained at ultrashort timescale by two-photon-absorption (TPA) in a semiconductor photon-counting module. A characteristic spectrum, due to the interference in multi-mode fiber, is observed directly in TPA detector for the first time. To analyze the output of such measurement, a theoretical model based on the Feynman's path-integral theory is built, which makes the contribution of related item and the corresponding spectral component match very well. In addition, by introducing an all-optical method into the current HBT apparatus, one can obtain the concerned second-order coherence spectrum directly without any postprocessing. This result may be helpful to develop ultrafast detection for the intensity interferometer with natural light. Meanwhile, the observation of HBT effect of multi-mode interference offers a new detection method for the optical fiber sensors.

Index Terms: Hanbury Brown and Twiss effect, two-photon-absorption detection, Feynman's path-integral theory.

1. Introduction

In 1956, two-photon bunching was first observed by Hanbury Brown and Twiss, in which randomly emitted photons by thermal light source were found to have the tendency to come in bunching rather than random [1]–[3]. Their experimental setup, known as Hanbury Brown and Twiss (HBT) interferometer, plays an important role in the second-order coherence light and photon statistics in quantum optics [4], [5]. HBT effect as the second-order measurement of intensity correlation has special advantages. Especially, it can be used to demonstrate two-photon bunching and apply in ghost imaging [6]–[17]. Here, the key of HBT measurement is that the intensity fluctuation of light

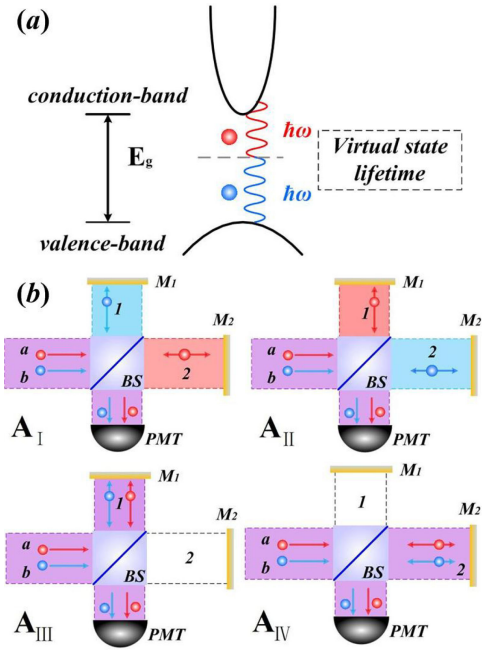

Fig. 1. The schematic diagrams of TPA and four paths to trigger detector for two photons. (a) shows that two photons are absorbed by a direct-gap semiconductor. If two photons reach in the virtual state lifetime, the TPA transition can occur. (b) shows that two independent photons *a* and *b* have four alternative ways to trigger the GaAs photomultiplier tube (PMT). BS is a 50:50 beam splitter.

needs to be obtained. However, for thermal light, e.g., sunlight, the intensity fluctuation is too fast (∼fs) to be detected directly by the current photodiode detector.

Lots of techniques have been proposed to alleviate the detector time constraint, where HBT apparatus composed of an interferometry apparatus (e.g., Michelson interferometer or Mach-Zehnder interferometer) with two-photon absorption (TPA) in a semiconductor photon-counting module is one of the most feasible methods [18]–[21]. In the TPA detector, a nonlinear optical effect would occur when a pair of photons are absorbed. The absorbing time is corresponding to $\hbar/E_g$ as the Heisenberg time as shown in Fig. 1(a). Here, $\hbar$ is the reduced Planck constant and E_g is the energy of bandgap. The rate of absorbing makes that the TPA detector can obtain the signal on the order of a few femtosecond. In this way, many groups have measured the intensity correlation and statistical properties of source, such as the bunching effect [22]–[26] and the ghost imaging [27]–[30] with the thermal light, and entangled photon-pairs [31]–[36]. Its vigor and vitality are being gradually shown. As mentioned above, researches are mainly focus on two cases: (1) Measure the time correlation of single-spatial-mode thermal light. In this case, the concerned measurement of the second-order coherence spectrum is accompanied by the high frequency oscillating terms and other unwanted spectral component. Usually, a postprocessing method by electronic filtering is employed to pick out the concerned second-order spectrum[19], [20], [22]–[25], [31]–[33]. (2) Based on the first case, imaging techniques such as ghost imaging are developed by measuring the spatial correlation of fluctuated multi-spatial-mode thermal light. Our work is to extend case (1) to the multi-spatial-mode thermal light, where a novel second-order coherence spectrum is presented.

In this paper, we report the HBT effect of multi-spatial-mode thermal light at ultrashort timescale by two-photon absorption in a semiconductor photon-counting module.We firstly employ quantum Feynman's path-integral theory to analyze the output of such measurement setup. The contribution of related items and the corresponding spectral components are matched. Based on such analysis, we find one can obtain the concerned second-order coherence spectrum directly without any postprocessing. Thus, by introducing an all-optical method into the current HBT apparatus, the

improved setup can measure directly the second-order spectra of thermal light from the single-mode fiber and the multi-mode fiber, respectively. Especially, the multi-mode HBT effect of thermal light, due to the interference in multi-mode fiber, is observed directly in TPA detector for the first time. The experimental results are agreement with the theoretical predictions well. This result may be helpful to develop ultrafast detection for the intensity interferometer with natural light. Meanwhile, the observation of HBT effect of multi-mode interference offers a new detection method for the optical fiber sensors.

This paper is organized as follows: at first we build a theoretical model based on Feynman's path-integral theory in Section 2. Experiments and discussion about results, which can show the HBT effect directly by an improved apparatus, are then given in Section 3. Section 4 summaries the conclusions.

2. Theory

The transition rate of TPA is related to the expectation value of [31]

$$\left\langle E^{(-)}(t)E^{(-)}(t+\tau)E^{(+)}(t+\tau)E^{(+)}(t)\right\rangle. \tag{1}$$

It is related to $I^2(\tau)$ [18]–[20] in photon counting regime of the classical theory.

From the quantum mechanical point of view, the signal of TPA in Eq. (1) can be calculated by the probability amplitude [5], [38]–[40], [42]. The original HBT effect can be interpreted as the coherent superposition of two probability amplitudes, nonclassical entities corresponding to different yet indistinguishable alternative ways of triggering a two-photon joint-detection event. In a similar way, our process can be thought that it is from a coherent superposition of four different yet indistinguishable probability amplitudes in the Michelson interferometer, as shown in Fig. 1(b).

Two independent photons (a and b) emitted by a thermal light source trigger a TPA detector (PMT) via four different Feynman's paths. The probability of observing a TPA detection event is determined by the superposition of these four two-photon amplitudes. As shown in Fig. 1(b), the channel in which photons are reflected by BS and M_1 is denoted as the channel 1, and the channel in which photons pass through BS and are reflected by M_2 is the channel 2. If the photon a (b) enters the channel, the channel is labeled as red (blue) as the color of photon a (b) is. If both photons enter the same channel, the channel is purple as the color overlay between red and blue. The white represents that no photon enters. When two mirrors (M_1 and M_2) are the same distance from the detector, four amplitudes superpose constructively. $G^{(2)}(\tau)$ achieves its maximum value due to constructive interference. When delay is not zero and less than the coherence time of light, the value of $G^{(2)}(\tau)$ will decrease. When delay is longer than the coherence time of light, the value of $G^{(2)}(\tau)$ is a constant due to that the paths are distinguishable in principle. For example, in the first case, photon a passes through BS and reaches M_2. At the same time, photon b is reflected by BS and reaches M_1. Finally, two photons, which are combined when they reach BS again, trigger the detector and achieve the TPA in the Heisenberg time. This is one way to trigger a TPA detection event, named as probability amplitude A_{I} as shown in Fig. 1(b). The definitions of other probability amplitudes are similar. The probability of a TPA detection event happening is the modulus square of the sum of all four probability amplitudes [5], [6], [37]–[42],

$$C_{TPA} \propto \left|A_{\mathrm{I}} + A_{\mathrm{II}} + A_{\mathrm{III}} + A_{\mathrm{IV}}\right|^2. \tag{2}$$

Based on Feynman's path-integral theory, four paths are *in principle* indistinguishable from each other in Eq. (2). Here, to distinguish the way of triggering detector from the symbol, A_{I} can be written as A_{a2b1}, where the subscript $a2b1$ represents that photon a propagates in the channel 2 and photon b propagates in the channel 1. In a similar way, other symbols can be written as A_{a1b2}, A_{a1b1} and A_{a2b2}, respectively. A_{aibj} can be written as

$$A_{aibj} = e^{i\varphi_a}e^{-i\omega_a(t_i-t_a)}\left|\varphi_a\right\rangle e^{i\varphi_b}e^{-i\omega_b(t_j-t_b)}\left|\varphi_b\right\rangle, \tag{3}$$

where $i, j = 1, 2$ and $t_{i,j}$ denotes the time of triggering detector when photon is reflected by $M_{i,j}$. When all amplitudes are represented by Eq. (3), Eq. (2) can be written as

$$C_{TPA} \propto (A_{a1b2} + A_{a2b1} + A_{a1b1} + A_{a2b2}) \times (A^*_{a1b2} + A^*_{a2b1} + A^*_{a1b1} + A^*_{a2b2}). \quad (4)$$

Consequently, Eq. (4) contains 16 items and can be calculated as (detailed calculation can be seen in Appendix A)

$$C_{TPA} \propto 1 + 1 + \mathrm{sinc}^2\left(\frac{1}{2}\Delta\omega\tau\right) + \cos(2\omega_0\tau)\,\mathrm{sinc}^2\left(\frac{1}{2}\Delta\omega\tau\right) + 4\cos(\omega_0\tau)\,\mathrm{sinc}\left(\frac{1}{2}\Delta\omega\tau\right), \quad (5)$$

where $1 + \mathrm{sinc}^2(\frac{1}{2}\Delta\omega\tau)$ is corresponding to $G^{(2)}(\tau)$. In Eq. (5), $1 + 1$ is the contribution from the interference of the same probability amplitude; $\mathrm{sinc}^2(\frac{1}{2}\Delta\omega\tau)$ is the contribution from the interference between the different probability amplitudes when photons *a* and *b* propagate in the separate channels; $\cos(2\omega_0\tau)\mathrm{sinc}(\frac{1}{2}\Delta\omega\tau)$ is the contribution from the interference between the different probability amplitudes when photons *a* and *b* propagate in the same channel; $\cos(\omega_0\tau)\mathrm{sinc}(\frac{1}{2}\Delta\omega\tau)$ is the contribution from the interference between the probability amplitude when photons *a* and *b* propagate in the separate channels and the probability amplitude when photons *a* and *b* propagate in the same channel.

In Eqs. (A1)–(A7) and (5), it can be found that the sinc-function comes from the rectangular frequency spectrum. When the type of the spectrum distribution of light source $f(\omega)$ changes, the calculation process is more complex and the sinc-function would be replaced by the new type of function in the Eq. (5). When the light source with the Gaussian spectrum distribution is employed, $f(\omega)$ becomes a Gaussian function. It is practical and convenient to assume a Gaussian spectrum of

$$f(\omega) = \frac{1}{\sqrt{2\pi}\Delta\omega} e^{-\frac{(\omega-\omega_0)^2}{2(\Delta\omega)^2}}. \quad (6)$$

All items are re-calculated. When all of 16 items are obtained and summed, the result can be obtained as (detailed calculation can be seen in Appendix B)

$$C_{TPA} \propto 1 + 1 + e^{-(\Delta\omega)^2\tau^2} + \cos(2\omega_0\tau)e^{-(\Delta\omega)^2\tau^2} + 4\cos(\omega_0\tau)e^{-\frac{(\Delta\omega)^2\tau^2}{2}}. \quad (7)$$

In fact, Eqs. (A2), (A4) and (A6) show that the calculation is similar to the process of Fourier Transformation (FT). The sinc-shaped profile can be obtained due to the FT of the rectangular function. When the type of the spectrum distribution of light source $f(\omega)$ changes, the process of calculation for Eq. (5) would become more complex and the sinc-function would be replaced by FT of the new function of spectrum distribution. As shown in Eqs. (B1) and (7), when the light source with the Gaussian spectrum distribution is employed, the sinc-function in Eq. (5) would be replaced by the Gaussian function due to the fact that the FT of Gaussian function is still Gaussian shape. However, the ratio for each item and its contribution from probability amplitudes are same in Eqs. (5) and (7).

The value by Feynman's path-integral theory is corresponding to the value of $I^2(\tau)$ by calculating in classical theory [19], [22], [25].

3. Experiments and Discussion

The experimental setup is shown in Fig. 2. The light is emitted from the amplified spontaneous emission (ASE) source with a center wavelength of 1550 nm and enters a standard Michelson interferometer. A H7421-50 Hamamatsu GaAs photomultiplier tube is employed in which the wavelength of TPA ranges from 900 to 1800 nm. The dark count is 60 per second. Firstly, the experiment

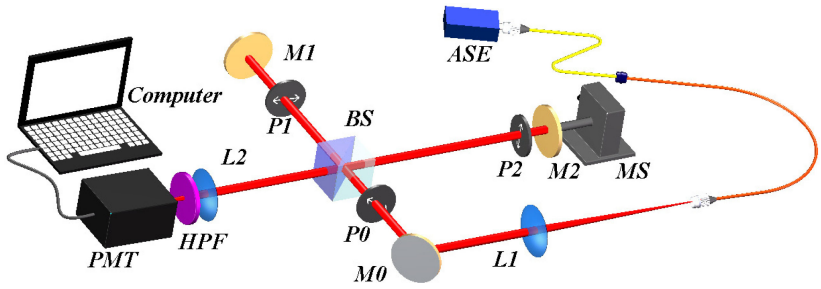

Fig. 2. The scheme of experiment. Light is emitted by an ASE source through fiber and enters a standard Michelson interferometer. ASE: amplified spontaneous emission, L_1: 100 mm lens, L_2: 25.4 mm lens, BS: 50:50 beam splitter, HPF: 1300 nm high-pass filter, M_0, M_1 and M_2: high reflection mirrors, MS: motorized stage, PMT: TPA detector, P_0, P_1 and P_2: polarizers. M_2 can move forward and back to change the time delay.

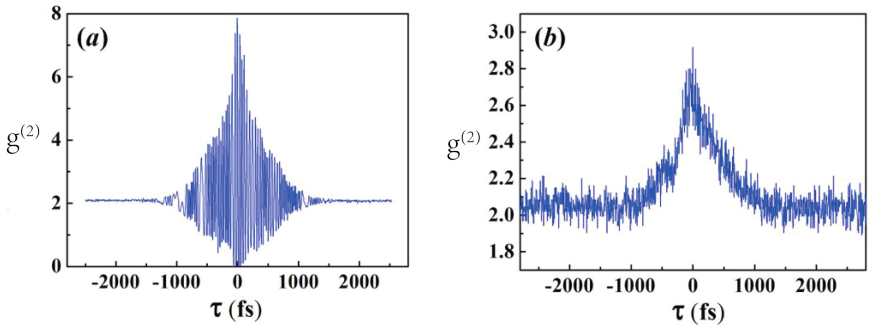

Fig. 3. The results about the temporal HBT effect. (a) shows the result of counts in TPA. No polarizers are used. The visibility of the peak is about 97%. (b) shows the result when three polarizers are employed to filter out the oscillation items by all-optical method. The result shows that the concerned HBT effect can be observed directly. The FWHM is about 832 fs. The visibility of the peak is about 15%.

scheme is tested and the HBT effect at ultrashort timescale is observed. All polarizers shown in Fig. 2 are not used in this step. Going through a single-mode fiber, the light enters such HBT apparatus. It is split into two beams by a 50:50 beam splitter (BS). Two beams propagate in two arms of Michelson interferometer and are reflected by two mirrors, respectively. When they reach BS again, they are combined in one beam. Because the counts of TPA are inversely proportional to the spot area of the light on the detector, a lens is employed to get a smaller spot area. An 1300 nm high-pass filter is used to filter out radiation wavelengths shorter than 1300 nm in the incident light. It aims to make that the one-photon counts of detector is close to zero as possible. At last, this beam triggers the detector through the lens and high-pass filter.

Figure 3(a) shows the result by the typical HBT set-up with a TPA detector. The full width at half-maximum (FWHM) is about 790 fs. It contains $G^{(2)}(\tau)$ and other items as oscillation. When the oscillation items are filtered out by the way of signal postprocessing, $G^{(2)}(\tau)$ can be observed [19], [20], [22]–[25], [31], [32]. The value in Fig. 3(a) is related to contributions of all items in Eq. (5). In the matter of fact, Eq. (5) shows that C_{TPA} is composed of four kinds components. When the results in Eq. (5) are simulated, the contributions of four kinds would be observed in Fig. 4: (a) shows a constant, (b) is related to $G^{(2)}(\tau)$, (c) is the periodical oscillation with the center frequency ω_0, and the last (d) is the other periodical oscillation with the center frequency $2\omega_0$. $\Delta\omega$ is the frequency bandwidth of ASE source. Their complex spectrum is shown in Fig. 4(e) which corresponds to the result in Fig. 3(a).

Next, three polarizers are employed in Fig. 2. P_0 is set to 45° with respect to the horizontal polarization. Since ASE beam is fully unpolarized, only the light with 45° polarization can be

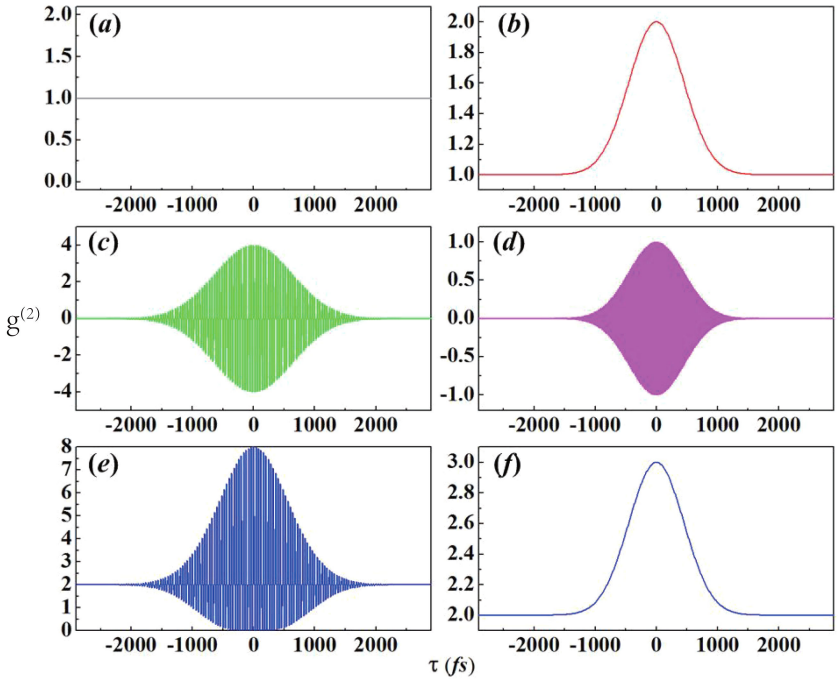

Fig. 4. The simulated results of Eq. (5) where the spectrum distribution of the light is Gaussian distribution. (a) shows the constant 1. (b) is related to $G^{(2)}(\tau)$. (c) shows the periodical oscillation with the center frequency ω_0. (d) shows the periodical oscillation with the center frequency $2\omega_0$. (e) shows the result combined with all items. (f) shows the sum of items when three polarizers are used.

selected. P_1 and P_2 are inserted in two arms. P_1 is set to the horizontal polarization and P_2 is set to the vertical polarization, respectively. Then, the beam is split into two beams by BS propagating in two arms. When two beams come back to BS, their polarization states would be filtered twice by P_1 and P_2, respectively. The polarization of the beam reflected by M_1 becomes horizontal. In the similar way, the other beam is the vertical polarization. The combined beam triggers the detector and the results are shown in Fig. 3(b). It comes from the coaction by $G^{(2)}(\tau)$ and the constant, where the background is thermal background which equals 2, not laser background which equals 1. To analyze the effects of polarizers in detail, the vector of polarization is employed. After the first polarizer, the light gets the 45° polarization which is represented as $[1/\sqrt{2}, 1/\sqrt{2}]^T$. Here $[1, 0]^T$ is corresponding to the horizontal polarization and $[0, 1]^T$ is the vertical polarization. When the beam passed through P_1, the polarization becomes horizontal and the vector becomes to $[1, 0]^T$. Similarly, it is easily understood that the polarization becomes vertical and the vector becomes to $[0, 1]^T$ when it passes P_2. Based on Feynman's path-integral theory, the result C_{TPA} is determined by the sum of $A_{aibj}A^*_{ai'bj'}$. i, j and i', j' are the channel which photons enter. Enter the channel 1 with P_1 and the photon gets the vector $[1, 0]^T$ in equation. Enter the channel 2 with P_2 and the photon gets $[0, 1]^T$. In this way, Eq. (3) would introduce the polarization vector as the modified factor. When Eq. (5) is calculated again, some items are filtered out due to $[1, 0]^T[0, 1] = 0$.

For the first type, taking $A_{a1b2}A^*_{a1b2}$ for example, it can be written as

$$\begin{aligned} A_{a1b2}A^*_{a1b2} = \iint & f(\omega_a)f(\omega_b)e^{j\varphi_a}e^{-i\omega_a(t_1-t_a)}[1, 0]^T e^{j\varphi_b} \\ & \times e^{-i\omega_b(t_2-t_b)}[0, 1]^T e^{-i\varphi_a}e^{j\omega_a(t_1-t_a)}[1, 0]e^{-i\varphi_b} \\ & \times e^{j\omega_b(t_2-t_b)}[0, 1]d\omega_a d\omega_b. \end{aligned} \tag{8}$$

Because the product of $[1,0]^T, [0,1]^T, [1,0]$ and [0,1] is 1, this item survives. It comes from the interference of the same probability amplitude. In such case, four items belong to this type and can survive.

For the second type, taking $A_{a1b2}A^*_{a2b1}$ for example, it can be written as

$$A_{a1b2}A^*_{a2b1} = \iint f(\omega_a)f(\omega_b)e^{j\varphi_a}e^{-i\omega_a(t_1-t_a)}[1,0]^T e^{j\varphi_b} \times e^{-i\omega_b(t_2-t_b)}[0,1]^T e^{-i\varphi_a}e^{j\omega_a(t_2-t_a)}[0,1]e^{-i\varphi_b} \times e^{j\omega_b(t_1-t_b)}[1,0]d\omega_a d\omega_b. \quad (9)$$

Since the product of $[1,0]^T, [0,1]^T, [0,1]$ and [1,0] is 1, this item survives. This comes from the interference of the different probability amplitude when two photons propagate in separate channels. Thus, two items belong to this type and can survive.

For the third type, such as $A_{a1b2}A^*_{a1b1}$, this item can be written as

$$A_{a1b2}A^*_{a1b1} = \iint f(\omega_a)f(\omega_b)e^{j\varphi_a}e^{-i\omega_a(t_1-t_a)}[1,0]^T e^{j\varphi_b} \times e^{-i\omega_b(t_2-t_b)}[0,1]^T e^{-i\varphi_a}e^{j\omega_a(t_1-t_a)}[1,0]e^{-i\varphi_b} \times e^{j\omega_b(t_1-t_b)}[1,0]d\omega_a d\omega_b. \quad (10)$$

This item is filtered out due to the fact that the product of $[1,0]^T, [0,1]^T, [1,0]$ and [1,0] is $[0,1]^T[1,0] = 0$. It comes from the interference between the probability amplitude when two photons propagate in two separate channels and the probability amplitude when two photons propagate in the same channel. Therefore, the first two vectors and last two vectors are always different in this type. Finally, eight items belong to this type and are filtered out.

For the fourth type, such as $A_{a1b1}A^*_{a2b2}$, this item can be written as

$$A_{a1b1}A^*_{a2b2} = \iint f(\omega_a)f(\omega_b)e^{j\varphi_a}e^{-i\omega_a(t_1-t_a)}[1,0]^T e^{j\varphi_b} \times e^{-i\omega_b(t_1-t_b)}[1,0]^T e^{-i\varphi_a}e^{j\omega_a(t_2-t_a)}[0,1]e^{-i\varphi_b} \times e^{j\omega_b(t_2-t_b)}[0,1]d\omega_a d\omega_b. \quad (11)$$

The product of $[1,0]^T, [1,0]^T, [0,1]$ and [0,1] is 0 due to $[1,0]^T[0,1] = 0$. It comes from the interference of the different probability amplitude when two photons propagate in the same channel. So the first two vectors and last two vectors are always different. Two items belong to this type and are filtered out.

Consequently, only 6 of all 16 items survive. The result is shown in Fig. 3(b) and the HBT effect with mutual-orthogonal polarizations is observed directly.

In reference [25], the light with mutual-orthogonal polarizations triggers the TPA detector and no HBT effect is observed. They also used P_1 and P_2 in the same location. A constant is shown in their result. The important key what we can successfully observe such HBT effect is the P_0. In fact, the peak of $G^{(2)}(\tau)$ is determined by the indistinguishable two-photon paths. If at the beginning the photon *a* has the horizontal polarization and the photon *b* has the vertical polarization, they are distinguishable in principle. There is only one path to trigger the detector for two photons *a* and *b*. Photon *a* can only enter the channel 1, while photon *b* can only enter the channel 2. In this case, HBT effect can not be observed. The value of $G^{(2)}(\tau)$ is a constant. In our experiment, P_0 makes that photons *a* and *b* have the same polarization, they are indistinguishable before they enter the Michelson interferometer. There are still four paths to trigger the detector and Eq. (5) can be hold. The result differing from their's is that the concerned $G^{(2)}(\tau)$ and constant are left. Especially, because the counts of detector contain these two styles of components at the same time, the peak visibility would become lower than the one of a pure $G^{(2)}(\tau)$.

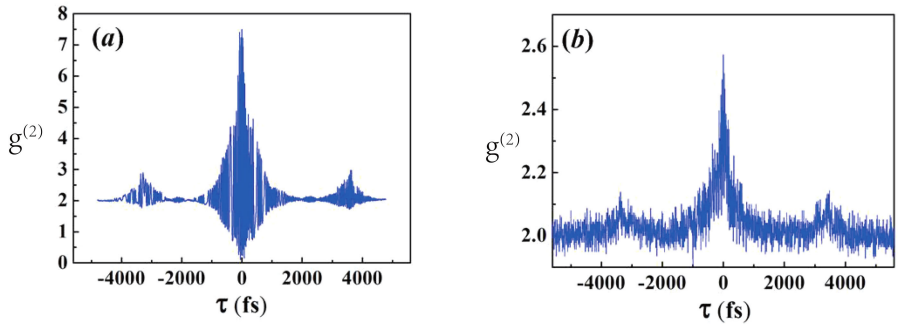

Fig. 5. The results about the temporal HBT effect with the multi-mode fiber. (a) shows the counts in TPA when the multi-mode fiber is employed. No polarizers are used. (b) shows the result when the items of periodical oscillation are filtered out by the improved HBT setup. The result shows that three HBT effects can be observed.

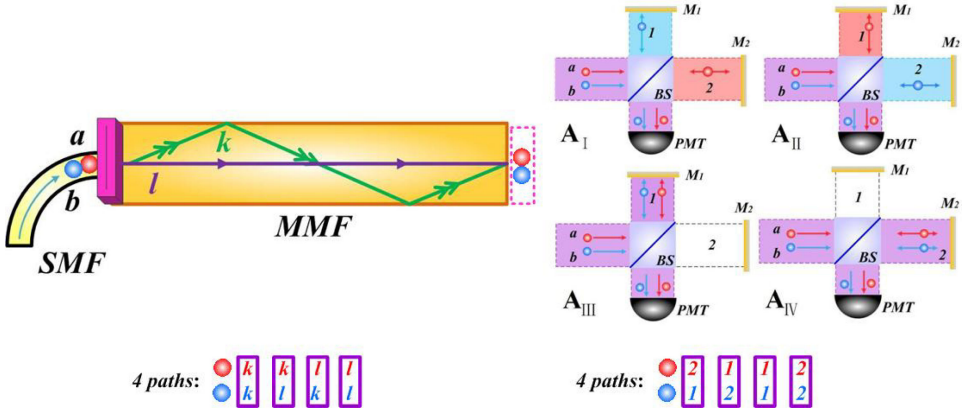

Fig. 6. Two independent photons *a* and *b* have 16 alternative paths to trigger the TPA detector when a multi-mode fiber is used. Left panel: two propagating channels *k* and *l* inside the multi-mode fiber are selected for photons. The time for photons along channel *k* is τ_0 longer than the time along channel *l*. 4 paths (*kk*, *ll*, *kl*, *lk*) passing the multi-mode fiber are selected. Right panel: 4 paths in the Michelson interferometer. The new four two-photon amplitudes would change the probability of observing a TPA detection event.

In the next experiment, by applying such improved HBT apparatus, the second-order spectrum of different spatial mode of thermal light going through a multi-mode fiber is directly observed. Here, a multi-mode fiber connected behind the single-mode fiber is used to generate a multi-mode thermal light. The interference between multi-mode leads to a novel result. As the spatial mode increases, besides the above result, there two side peaks of the HBT effect are observed. The result without polarizers is shown in Fig. 5(a). The visibility of the main peak is about 97%. The FWHM of the main peak is about 712 fs. The visibility of the left peak is 24%. Its distance to the main peak is about 3300 fs. The FWHM is about 871 fs. The visibility of the right peak is 26%. Its distance to the main peak is about 3400 fs. The FWHM is about 881 fs.

When the light enters the multi-mode fiber from the single-mode fiber, multi-modes would be generated. The number of mode is determined by fiber parameters. More modes can be considered as the multi-mode fiber offers more paths for photons to trigger the detector. Based on Feynman's path-integral theory, the more superposition of paths would occur. To explain this effect, two modes inside the multi-mode fiber are selected as the model. As shown in the left panel of Fig. 6, two propagation channels *k* and *l* in multi-mode fiber can be selected for photons. The time when photons go through the fiber along channel *k* is τ_0 longer than the time of channel *l*. For two photons

a and *b*, there are 4 paths passing the multi-mode fiber: *a* and *b* pass through the channel *k* together, *a* and *b* pass through the channel *l* together, *a* passes through the channel *k* and *b* passes through the channel *l*, *b* passes through the channel *k* and *a* passes through the channel *l*, respectively. If these 4 paths in the multi-mode fiber combine with 4 paths in the Michelson interferometer, there are totally 16 paths for the photons *a* and *b* to trigger the TPA detector together. Equation (2) would be rewritten as

$$C_{TPA} = \left| \sum_{i=1}^{n} A_i \right|^2, n = 16. \tag{12}$$

Here, to distinguish the way of triggering detector from the symbol, A_1 can be written as A_{ak2bl1}, which is similar to Eq. (3). *ak*2*bl*1 represents that photon *a* propagates in the channel *k* and photon *b* propagates in the channel *l* when they pass through the multi-mode fiber. Then when two photons enter the Michelson interferometer to trigger the TPA detector, photon *a* propagates in the channel 2 and photon *b* propagates in the channel 1. A_{axibyj} can be written as

$$A_{axibyj} = e^{j\varphi_a} e^{-i\omega_a(t_x+t_i)} \left|\varphi_a\right\rangle e^{j\varphi_b} e^{-i\omega_b(t_y+t_j)} \left|\varphi_b\right\rangle, \tag{13}$$

where $x, y = k, l$ and $t_{x,y}$ represents the time for photon propagating in channel x, y in the multi-mode fiber. $i, j = 1, 2$ and $t_{i,j}$ represents the time for photon propagating in channel i, j in the Michelson interferometer. The number of A_{axibyj} is 16. When all amplitudes are represented by Eq. (13), there are 256 items in Eq. (12). Every item is the product of two probability amplitudes. Two probability amplitudes can be represented by A_{axibyj} and $A_{ax'i'by'j'}$. One item can be written as

$$\begin{aligned} A_{axibyj} A^*_{ax'i'by'j'} &= \iint f(\omega_a) f(\omega_b) e^{j\varphi_a} e^{j\varphi_b} e^{-i\omega_a(t_x+t_i)} e^{-i\omega_b(t_y+t_j)} \\ &\quad \times e^{-i\varphi_a} e^{-i\varphi_b} e^{j\omega_a(t_{x'}+t_{i'})} e^{j\omega_b(t_{y'}+t_{j'})} d\omega_a d\omega_b \\ &= \iint f(\omega_a) f(\omega_b) e^{j\omega_a[(t_{i'}-t_i)+(t_{x'}-t_x)]} \\ &\quad \times e^{j\omega_b[(t_{j'}-t_j)+(t_{y'}-t_y)]} d\omega_a d\omega_b. \end{aligned} \tag{14}$$

In Eq. (14), $f(\omega)$ is the spectrum distribution of the source, which is similar to Eq. (A1). Since the spectrum distribution doesn't influence the contribution from every path, the similar approximation is used here and the spectrum distribution is still thought as the rectangular frequency spectrum. The center frequency is ω_0 and the bandwidth of frequency is $\Delta\omega$. By the similar process of simplification in Eqs. (A4) and (A6), Eq. (14) can be written as

$$\begin{aligned} A_{axibyj} A^*_{ax'i'by'j'} &= \int_{\omega_0-\frac{1}{2}\Delta\omega}^{\omega_0+\frac{1}{2}\Delta\omega} 1 \cdot e^{j\omega_a[(t_{i'}-t_i)+(t_{x'}-t_x)]} d\omega_a \\ &\quad \times \int_{\omega_0-\frac{1}{2}\Delta\omega}^{\omega_0+\frac{1}{2}\Delta\omega} 1 \cdot e^{j\omega_b[(t_{j'}-t_j)+(t_{y'}-t_y)]} d\omega_b \\ &\propto (\Delta\omega)^2 e^{j\omega_0[(t_{i'}-t_i)+(t_{x'}-t_x)]} e^{j\omega_0[(t_{j'}-t_j)+(t_{y'}-t_y)]} \\ &\quad \times \operatorname{sinc} \frac{\Delta\omega[(t_{i'}-t_i)+(t_{x'}-t_x)]}{2} \\ &\quad \times \operatorname{sinc} \frac{\Delta\omega[(t_{j'}-t_j)+(t_{y'}-t_y)]}{2}. \end{aligned} \tag{15}$$

For $A_{axibyj} A_{ax'i'by'j'}$, there are 256 items due to $i = (1, 2)$, $i' = (1, 2)$, $x = (k, l)$, $x' = (k, l)$, $j = (1, 2)$, $j' = (1, 2)$, $y = (k, l)$ and $y' = (k, l)$. τ is employed to replace $t_2 - t_1$ and τ_o is employed to replace $t_k - t_l$. When all $(i, i', x, x', j, j', y, y')$ are traversed, $t_{i'} - t_i = (0, \pm\tau)$, $t_{j'} - t_j = (0, \pm\tau)$, $t_{x'} - t_x = (0, \pm\tau_o)$ and $t_{y'} - t_y = (0, \pm\tau_o)$ are substituted into Eq. (15) and all items are obtained.

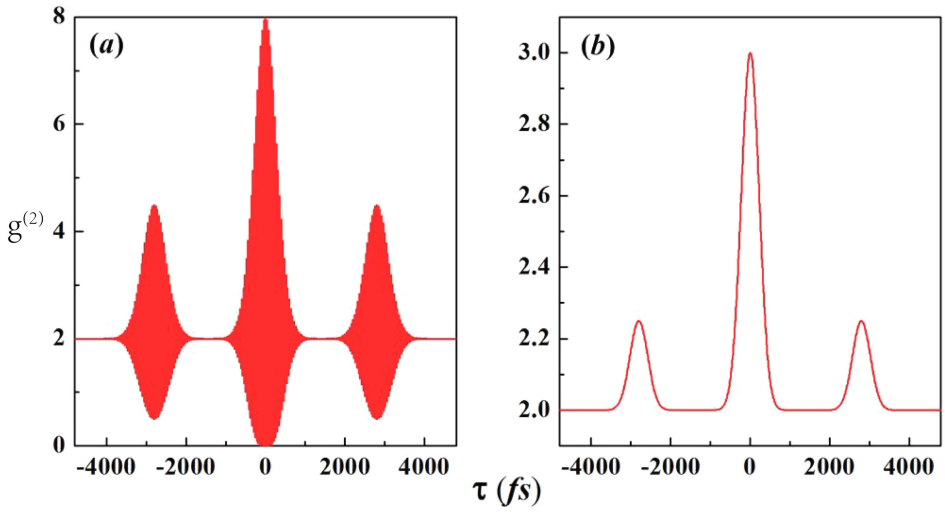

Fig. 7. The simulated results in Eqs. (17) and (19) for the light source with the Gaussian spectrum distribution. (a) shows the result combined with all items in Eq. (17). (b) shows the results combined with left items when some items are filtered out by polarizers as Eq. (19).

When 256 items are summed, Eq. (12) is calculated as

$$C_{TPA} \propto \left\{2 + 2\cos(\omega_0\tau)\mathrm{sinc}\left(\frac{1}{2}\Delta\omega\tau\right) + \cos[\omega_0(\tau-\tau_0)]\mathrm{sinc}\left[\frac{1}{2}\Delta\omega(\tau-\tau_0)\right] + 2\cos(\omega_0\tau_0)\mathrm{sinc}\left(\frac{1}{2}\Delta\omega\tau_0\right) + \cos[\omega_0(\tau+\tau_0)]\mathrm{sinc}\left[\frac{1}{2}\Delta\omega(\tau+\tau_0)\right]\right\}^2. \quad (16)$$

When the light source with the Gaussian spectrum distribution is employed, the sinc-function would be replaced again by the Gaussian function due to that the FT of Gaussian function is still Gaussian shape. By the same process of calculation, Eq. (16) is written as

$$C_{TPA} \propto \left\{2 + 2\cos(\omega_0\tau)e^{-\frac{(\Delta\omega)^2\tau^2}{2}} + 2\cos(\omega_0\tau_0)e^{-\frac{(\Delta\omega)^2\tau_0^2}{2}} + \cos[\omega_0(\tau-\tau_0)]e^{-\frac{(\Delta\omega)^2(\tau-\tau_0)^2}{2}} + \cos[\omega_0(\tau+\tau_0)]e^{-\frac{(\Delta\omega)^2(\tau+\tau_0)^2}{2}}\right\}^2, \quad (17)$$

whose simulation is shown in Fig. 7(a).

When three polarizers are employed again, the HBT effect between different modes can be observed directly. The result is shown in Fig. 5(b). It shows that three HBT effects can be observed directly. The FWHMs of the main peak, left peak and right peak are 746 fs, 911 fs and 921 fs, respectively. The visibility of the main peak, left peak and right peak are 12.5%, 3.1% and 3.1%, respectively. 16 probability amplitudes in Eq. (12) is caused by 4 paths in the multi-mode fiber and 4 paths in the Michelson interferometer. As mentioned in Eqs. (8)–(11), the effect of polarizers makes that 10 of 16 items from 4 paths in the Michelson interferometer are filtered out. For $A_{axibyj}A_{ax'i'by'j'}$, the previous (i, i', j, j') can not be selected and 6 items survive in 16 items ($i = 1, 2; i' = 1, 2; j = 1, 2; j' = 1, 2$). The paths from the multi-mode fiber are not affected and theirs 16 items ($x = k, l; x' = k, l; y = k, l; y' = k, l$) are not changed. Consequently, only 6×16 of 16×16 items survive. When the

corresponding $(i, i', x, x', j, j', y, y')$ are selected and 96 items are summed, Eq. (16) would become to

$$\begin{aligned} C_{TPA} \propto\ & 8 + 4\mathrm{sinc}^2\left(\frac{1}{2}\Delta\omega\tau\right) + \mathrm{sinc}^2\left[\frac{1}{2}\Delta\omega(\tau-\tau_o)\right] \\ & + 16\cos\,(\omega_o\tau_o)\,\mathrm{sinc}\left(\frac{1}{2}\Delta\omega\tau_o\right) + 4\mathrm{sinc}^2\left(\frac{1}{2}\Delta\omega\tau_o\right) \\ & + 4\cos\,(\omega_o\tau_o)\mathrm{sinc}\left(\frac{1}{2}\Delta\omega\tau_o\right)\left\{\mathrm{sinc}\left[\frac{1}{2}\Delta\omega(\tau-\tau_o)\right]\right. \\ & \left. + \mathrm{sinc}\left[\frac{1}{2}\Delta\omega(\tau+\tau_o)\right]\right\} + \mathrm{sinc}^2\left[\frac{1}{2}\Delta\omega(\tau+\tau_o)\right] \\ & + 2\cos\,(2\omega_o\tau_o)\mathrm{sinc}^2\left(\frac{1}{2}\Delta\omega\tau_o\right) \\ & + 2\cos\,(2\omega_o\tau_o) \times \mathrm{sinc}\left[\frac{1}{2}\Delta\omega(\tau+\tau_o)\right]\mathrm{sinc}\left[\frac{1}{2}\Delta\omega(\tau-\tau_o)\right], \end{aligned} \tag{18}$$

The HBT effect of different modes can be observed directly. When $f(\omega)$ is the Gaussian spectrum distribution, Eq. (18) is written as

$$\begin{aligned} C_{TPA} \propto\ & 8 + 4e^{-(\Delta\omega)^2\tau^2} + e^{-(\Delta\omega)^2(\tau-\tau_o)^2} + 16\cos\,(\omega_o\tau_o)e^{-\frac{(\Delta\omega)^2\tau_o^2}{2}} \\ & + 4e^{-(\Delta\omega)^2\tau_o^2} + 2\cos\,(2\omega_o\tau_o)e^{-\frac{(\Delta\omega)^2(\tau+\tau_o)^2}{2}}e^{-\frac{(\Delta\omega)^2(\tau-\tau_o)^2}{2}} \\ & + 4\cos\,(\omega_o\tau_o)e^{-\frac{(\Delta\omega)^2\tau_o^2}{2}}\left[e^{-\frac{(\Delta\omega)^2(\tau-\tau_o)^2}{2}} + e^{-\frac{(\Delta\omega)^2(\tau+\tau_o)^2}{2}}\right] \\ & + e^{-(\Delta\omega)^2(\tau+\tau_o)^2} + 2\cos\,(2\omega_o\tau_o)e^{-(\Delta\omega)^2\tau_o^2}, \end{aligned} \tag{19}$$

whose simulation is shown in Fig. 7(b).

In Eqs. (16) and (18), τ_o determines the location of the left and right peak. It is determined by the fiber parameters, such as the length and core diameter. The simulated results in Fig. 7 is caused by two modes. When the number of modes in fiber increases, the calculation would become more complex and more sub-peaks can be observed in different locations. At the same time, their visibility are affected due to the different intensity of different modes.

4. Conclusion

In summary, firstly, the output of HBT apparatus via two-photon absorption in a semiconductor photon-counting module is analyzed by Feynman's path-integral theory. The contribution of related items and the corresponding spectral component are presented. The analysis shows that the concerned item can be picked out without any postprocessing by means of the all-optical methods. To verify our prediction, an improved setup is strategically arranged by introducing an all-optical method into the current HBT apparatus. We have directly measured the second-order spectra of thermal light from the single-mode fiber and the multi-mode fiber, respectively. And the multi-mode HBT effect of thermal light, due to the interference in multi-mode fiber, is observed directly in TPA detector for the first time. The experimental results are well agreement with the theoretical predictions. The new interpretation and the all-optical method of directly observing HBT effect help a whole thorough understanding into the HBT effect in TPA detector. It can also lead to interesting studies by exploring new HBT effect at femtosecond timescale.

Meanwhile, the optical fiber sensors based on multi-mode interference have been developed fast in recent years. Compared with traditional optical fiber sensors, the distinctive advantages as simple structure, flexible design, widely sensing range and so on make them popular in more

and more fields [43]–[48]. The direct measurement of the HBT effect of multi-mode interference at the ultrashort timescale may offer a new detection method for the optical fiber sensors. As a new second-order correlation detection, it may be helpful for the development of the optical fiber sensors.

Appendix A
Calculations of the Probability of a TPA Detection Event Based on Feynman's Path-Integral Theory

There are 16 items when Eq. (4) is expanded to calculate. All items can be classified into four groups.

Firstly, for $A_{a1b2}A^*_{a1b2}$, the value is a constant because the probability amplitudes times its complex conjugate. 4 of 16 items belong to this type, which come from the interference between the same probability amplitude.

Secondly, for $A_{a1b2}A^*_{a2b1}$, this item can be written as

$$\begin{aligned} A_{a1b2}A^*_{a2b1} &= \iint f(\omega_a)f(\omega_b)e^{j\varphi_a}e^{j\varphi_b}e^{-i\omega_a(t_1-t_a)}e^{-i\omega_b(t_2-t_b)} \\ &\quad \times e^{-i\varphi_a}e^{-i\varphi_b}e^{i\omega_a(t_2-t_a)}e^{i\omega_b(t_1-t_b)}d\omega_a d\omega_b \\ &= \iint f(\omega_a)f(\omega_b)e^{-i\omega_a(t_1-t_2)} \times e^{-i\omega_b(t_2-t_1)}d\omega_a d\omega_b, \end{aligned} \tag{A1}$$

where $f(\omega_a)$ and $f(\omega_b)$ are the spectrum distribution of light source. Set the center frequency is ω_0 and the frequency bandwidth is $\Delta\omega$. Equation A1 can be written as

$$A_{a1b2}A^*_{a2b1} = \int_{\omega_0-\frac{1}{2}\Delta\omega}^{\omega_0+\frac{1}{2}\Delta\omega} f(\omega_a)e^{-i\omega_a(-\tau)}d\omega_a \times \int_{\omega_0-\frac{1}{2}\Delta\omega}^{\omega_0+\frac{1}{2}\Delta\omega} f(\omega_b)e^{-i\omega_b\tau}d\omega_b, \tag{A2}$$

where $\tau = t_2 - t_1$.

For different light sources, the spectrum distribution can be rectangular function, Gaussian function or Lorentzian distribution function. Set the spectrum distribution $f(\omega)$ as the rectangular frequency spectrum, Eq. (A2) is written as

$$\begin{aligned} A_{a1b2}A^*_{a2b1} &= \int_{\omega_0-\frac{1}{2}\Delta\omega}^{\omega_0+\frac{1}{2}\Delta\omega} 1\cdot e^{-i\omega_a(-\tau)}d\omega_a \int_{\omega_0-\frac{1}{2}\Delta\omega}^{\omega_0+\frac{1}{2}\Delta\omega} 1\cdot e^{-i\omega_b\tau}d\omega_b \\ &= \frac{1}{\tau^2}\cdot e^{j\omega_a\tau}\Big|_{\omega_0-\frac{1}{2}\Delta\omega}^{\omega_0+\frac{1}{2}\Delta\omega} \cdot e^{-i\omega_b\tau}\Big|_{\omega_0-\frac{1}{2}\Delta\omega}^{\omega_0+\frac{1}{2}\Delta\omega} \\ &= (\Delta\omega)^2\mathrm{sinc}^2\left(\frac{1}{2}\Delta\omega\tau\right). \end{aligned} \tag{A3}$$

$A_{a2b1}A^*_{a1b2}$ is similar to $A_{a1b2}A^*_{a2b1}$ in the process of calculation, so 2 of 16 items belong to this type. They come from the interference between the different probability amplitude when photons a and b propagate in the separate channel.

Thirdly, for $A_{a1b2}A^*_{a1b1}$, this item can be written as

$$\begin{aligned} A_{a1b2}A^*_{a1b1} &= \iint f(\omega_a)f(\omega_b)e^{j\varphi_a}e^{j\varphi_b}e^{-i\omega_a(t_1-t_a)}e^{-i\omega_b(t_2-t_b)}e^{-i\varphi_a} \\ &\quad \times e^{-i\varphi_b}e^{j\omega_a(t_1-t_a)}e^{j\omega_b(t_1-t_b)}d\omega_a d\omega_b \\ &= \iint f(\omega_a)f(\omega_b)e^{-i\omega_b\tau}d\omega_a d\omega_b \\ &= \int_{\omega_0-\frac{1}{2}\Delta\omega}^{\omega_0+\frac{1}{2}\Delta\omega} 1\cdot d\omega_a \int_{\omega_0-\frac{1}{2}\Delta\omega}^{\omega_0+\frac{1}{2}\Delta\omega} 1\cdot e^{-i\omega_b\tau}d\omega_b \\ &= \Delta\omega\cdot\frac{1}{(-i\tau)}\cdot e^{-i\omega_b\tau}\Big|_{\omega_0-\frac{1}{2}\Delta\omega}^{\omega_0+\frac{1}{2}\Delta\omega} \\ &= e^{-i\omega_0\tau}(\Delta\omega)^2\mathrm{sinc}\left(\frac{1}{2}\Delta\omega\tau\right). \end{aligned} \tag{A4}$$

By the similar calculation, the result of $A^*_{a1b2}A_{a1b1}$ is $e^{j\omega_0\tau}(\Delta\omega)^2\mathrm{sinc}(\frac{1}{2}\Delta\omega\tau)$. Adding these two items, the result can be obtained as

$$\begin{aligned} A_{a1b2}A^*_{a1b1} + A^*_{a1b2}A_{a1b1} &= (\Delta\omega)^2\mathrm{sinc}\left(\frac{1}{2}\Delta\omega\tau\right)(e^{-i\omega_0\tau}+e^{j\omega_0\tau}) \\ &= 2\cos(\omega_0\tau)(\Delta\omega)^2\mathrm{sinc}\left(\frac{1}{2}\Delta\omega\tau\right). \end{aligned} \tag{A5}$$

Four pairs (8 items) of 16 items belong to this type. They come from the interference between the probability amplitude when photons *a* and *b* propagate in the same channel and the probability amplitude when photons *a* and *b* propagate in the separate channel.

Fourthly, for $A_{a1b1}A^*_{a2b2}$, this item can be written as

$$\begin{aligned} A_{a1b1}A^*_{a2b2} &= \iint f(\omega_a)f(\omega_b)e^{j\varphi_a}e^{j\varphi_b}e^{-i\omega_a(t_1-t_a)}e^{-i\omega_b(t_1-t_b)}e^{-i\varphi_a} \\ &\quad \times e^{-i\varphi_b}e^{j\omega_a(t_2-t_a)}e^{j\omega_b(t_2-t_b)}d\omega_a d\omega_b \\ &= \iint f(\omega_a)f(\omega_b)e^{j\omega_a\tau}e^{j\omega_b\tau}d\omega_a d\omega_b \\ &= \int_{\omega_0-\frac{1}{2}\Delta\omega}^{\omega_0+\frac{1}{2}\Delta\omega} 1\cdot e^{j\omega_a\tau}d\omega_a \int_{\omega_0-\frac{1}{2}\Delta\omega}^{\omega_0+\frac{1}{2}\Delta\omega} 1\cdot e^{j\omega_b\tau}d\omega_b \\ &= \frac{1}{\tau^2}\cdot e^{j\omega_a\tau}\Big|_{\omega_0-\frac{1}{2}\Delta\omega}^{\omega_0+\frac{1}{2}\Delta\omega}\cdot e^{j\omega_b\tau}\Big|_{\omega_0-\frac{1}{2}\Delta\omega}^{\omega_0+\frac{1}{2}\Delta\omega} \\ &= e^{j2\omega_0\tau}(\Delta\omega)^2\mathrm{sinc}^2\left(\frac{1}{2}\Delta\omega\tau\right). \end{aligned} \tag{A6}$$

Adding two items $A_{a1b1}A^*_{a2b2}$ and $A^*_{a1b1}A_{a2b2}$, the result can be obtained as

$$\begin{aligned} A_{a1b1}A^*_{a2b2} + A^*_{a1b1}A_{a2b2} &= (\Delta\omega)^2\mathrm{sinc}^2\left(\frac{1}{2}\Delta\omega\tau\right)(e^{-i2\omega_0\tau}+e^{j2\omega_0\tau}) \\ &= 2\cos(2\omega_0\tau)(\Delta\omega)^2\mathrm{sinc}^2\left(\frac{1}{2}\Delta\omega\tau\right). \end{aligned} \tag{A7}$$

The result of these two items are the contribution from the interference between the different probability amplitudes when photons *a* and *b* propagate in the same channel.

Appendix B
Calculations With the Gaussian Spectrum Distribution Based on Feynman's Path-Integral Theory

In (A1)–(A7) and (5), it can be found that the sinc-function comes from the rectangular frequency spectrum. When the type of the spectrum distribution of light source $f(\omega)$ changes, the calculation process is more complex and the sinc-function would be replaced by the new type function in the Eq. (5). When the light source with the Gaussian spectrum distribution is employed, $f(\omega)$ becomes a Gaussian function. It is practical and convenient to assume a Gaussian spectrum of

$$f(\omega) = \frac{1}{\sqrt{2\pi}\Delta\omega} e^{-\frac{(\omega-\omega_0)^2}{2(\Delta\omega)^2}}.$$

For $A_{a1b2}A^*_{a1b1}$, this item in Eq. (A4) can be rewritten as

$$\begin{aligned} A_{a1b2}A^*_{a1b1} &= \iint f(\omega_a)f(\omega_b)e^{-i\omega_b\tau}d\omega_a d\omega_b \\ &= \int_{-\infty}^{+\infty} \frac{1}{\sqrt{2\pi}\Delta\omega} e^{-\frac{(\omega_a-\omega_0)^2}{2(\Delta\omega)^2}} d\omega_a \\ &\quad \times \int_{-\infty}^{+\infty} \frac{1}{\sqrt{2\pi}\Delta\omega} e^{-\frac{(\omega_b-\omega_0)^2}{2(\Delta\omega)^2}} \cdot e^{-i\omega_b\tau} d\omega_b. \end{aligned} \tag{B1}$$

There are two integral terms in Eq. (B1). The first term is the integral for the normalized Gaussian function and its value is 1. After simplification the second term can written as

$$\int_{-\infty}^{+\infty} \frac{1}{\sqrt{2\pi}\Delta\omega} e^{-\frac{(\omega_b-\omega_0)^2}{2(\Delta\omega)^2}} \cdot e^{-i\omega_b\tau} d\omega_b = e^{-i\omega_o\tau} \cdot e^{-\frac{(\Delta\omega)^2\tau^2}{2}}. \tag{B2}$$

Then $A_{a1b2}A^*_{a1b1}$ in Eq. (B1) would become to

$$A_{a1b2}A^*_{a1b1} = e^{-i\omega_o\tau} \cdot e^{-\frac{(\Delta\omega)^2\tau^2}{2}}. \tag{B3}$$

By the similar calculation, the result of $A^*_{a1b2}A_{a1b1}$ is $e^{i\omega_o\tau} \cdot e^{-\frac{(\Delta\omega)^2\tau^2}{2}}$. Adding these two items the result can be obtained as

$$\begin{aligned} A_{a1b2}A^*_{a1b1} + A^*_{a1b2}A_{a1b1} &= (e^{-i\omega_o\tau} + e^{i\omega_o\tau}) \cdot e^{-\frac{(\Delta\omega)^2\tau^2}{2}} \\ &= 2\cos\omega_o\tau e^{-\frac{(\Delta\omega)^2\tau^2}{2}}. \end{aligned} \tag{B4}$$

In a similar way to the above calculation of sinc-function, four pairs (8 items) of 16 items belong to this type.

For $A_{a1b2}A^*_{a2b1}$ in Eq. (A2), this item can be written as

$$\begin{aligned} A_{a1b2}A^*_{a2b1} &= \int_{-\infty}^{+\infty} \frac{1}{\sqrt{2\pi}\Delta\omega} e^{-\frac{(\omega_a-\omega_0)^2}{2(\Delta\omega)^2}} \cdot e^{-i\omega_a(-\tau)} d\omega_a \\ &\quad \times \int_{-\infty}^{+\infty} \frac{1}{\sqrt{2\pi}\Delta\omega} e^{-\frac{(\omega_b-\omega_0)^2}{2(\Delta\omega)^2}} \cdot e^{-i\omega_b\tau} d\omega_b \\ &= e^{-(\Delta\omega)^2\tau^2}. \end{aligned} \tag{B5}$$

2 of 16 items belong to this type. By the similar process, Eq. (A7) can be written as

$$\begin{aligned} A_{a1b1}A^*_{a2b2} + A^*_{a1b1}A_{a2b2} &= (e^{2i\omega_o\tau} + e^{-2i\omega_o\tau})e^{-(\Delta\omega)^2\tau^2} \\ &= 2\cos(2\omega_o\tau)e^{-(\Delta\omega)^2\tau^2}. \end{aligned} \tag{B6}$$

When all of 16 items are summed, the result can be obtained as

$$C_{TPA} \propto 1 + 1 + e^{-(\Delta\omega)^2\tau^2} + \cos(2\omega_0\tau)e^{-(\Delta\omega)^2\tau^2} + 4\cos(\omega_0\tau)e^{-\frac{(\Delta\omega)^2\tau^2}{2}}. \quad \text{(B7)}$$

References

[1] R. Hanbury Brown and R. Q. Twiss, "Correlation between photons in two coherent beams of light," *Nature*, vol. 177, pp. 27–29, 1956.
[2] R. Hanbury Brown and R. Q. Twiss, "A test of a new type of stellar interferometer on sirius," *Nature*, vol. 178, pp. 1046–1048, 1956.
[3] R. Hanbury Brown, *Intensity Interferometer.* London, U.K.: Taylor & Francis, 1974.
[4] L. Mandel and E. Wolf, *Optical Coherence and Quantum Optics.* New York, NY, USA: Cambridge Univ. Press, 1995., p. 714.
[5] M. O. Scully and M. S. Zubairy, *Quantum Optics.* New York, NY, USA: Cambridge Univ. Press, 1997.
[6] R. J. Glauber, "The quantum theory of optical coherence," *Phys. Rev.*, vol. 130, pp. 2529–2539, 1963.
[7] R. J. Glauber, "Coherent and incoherent states of the radiation field," *Phys. Rev.*, vol. 131, pp. 2766–2788, 1963.
[8] E. C. G. Sudarshan, "Equivalence of semiclassical and quantum mechanical descriptions of statistical light beams," *Phys. Rev. Lett.*, vol. 10, pp. 277–279, 1963.
[9] T. B. Pittman, Y. H. Shih, D. V. Strekalov, and A. V. Sergienko, "Optical imaging by means of two-photon quantum entanglement," *Phys. Rev. A*, vol. 52, pp. R3429–R3432, 1995.
[10] R. S. Bennink, S. J. Bentley, and R. W. Boyd, "Two-photon coincidence imaging with a classical source," *Phys. Rev. Lett.*, vol. 89, 2002, Art. no. 113601.
[11] A. Gatti, E. Brambilla, M. Bache, and L. A. Lugiato, "Ghost imaging with thermal Light: Comparing entanglement and classical correlation," *Phys. Rev. Lett.*, vol. 93, 2004, Art. no. 093602.
[12] J. Cheng and S. S. Han, "Incoherent coincidence imaging and its applicability in x-ray diffraction," *Phys. Rev. Lett.*, vol. 92, 2004, Art. no. 093903.
[13] D. Zhang, Y. H. Zhai, L. A. Wu, and X. H. Chen, "Correlated two-photon imaging with true thermal light," *Opt. Lett.*, vol. 30, pp. 2354–2356, 2005.
[14] Y. Cai and S. Y. Zhu, "Ghost imaging with incoherent and partially coherent light radiation," *Phys. Rev. E*, vol. 71, 2005, Art. no. 056607.
[15] K. W. C. Chan, M. N. O'Sullivan, and R. W. Boyd, "Optimization of thermal ghost imaging: High-order correlations vs. background subtraction," *Opt. Express*, vol. 18, pp. 5562–5573, 2010.
[16] Y. Zhou, J. Simon, J. B. Liu, and Y. H. Shih, "Third-Order correlation function and ghost imaging of chaotic thermal light in the photon counting regime," *Phys. Rev. A*, vol. 81, 2010, Art. no. 043831.
[17] Y. Shih, "The physics of ghost imaging: Nonlocal interference or local intensity fluctuation correlation?" *Quantum Inf. Process*, vol. 11, pp. 995–1001, 2012.
[18] B. R. Mollow, "Two-Photon absorption and field correlation functions," *Phys. Rev.*, vol. 175, pp. 1555–1563, 1968.
[19] K. Mogi, K. Naganuma, and H. Yamada, "A Novel real-time chirp measurement method for ultrashort optical pulses," *Jpn. J. Appl. Phys.*, vol. 27, pp. 2078–2081, 1988.
[20] J. M. Roth, T. E. Murphy, and Chris Xu, "Ultrasensitive and high-dynamic-range two-photon absorption in a GaAs photomultiplier tube," *Opt. Lett.*, vol. 27, pp. 2076–2078, 2002.
[21] A. Hayat, A. Nevet, P. Ginzburg, and M. Orenstein, "Applications of two-photon processes in semiconductor photonic devices: Invited review," *Semicond. Sci. Technol.*, vol. 26, 2011, Art. no. 083001.
[22] F. Boitier, A. Godard, E. Rosencher, and C. Fabre, "Measuring photon bunching at ultrashort timescale by two photon absorption in semiconductors," *Nature Phys.*, vol. 5, no. 4, pp. 267–270, 2009.
[23] A. Nevet, A. Hayat, and M. Orenstein, "Ultrafast pulse compression by semiconductor two-photon gain," *Opt. Lett.*, vol. 35, pp. 3877–3879, 2010.
[24] A. Nevet, A. Hayat, P. Ginzburg, and M. Orenstein, "Indistinguishable photon pairs from independent true chaotic sources," *Phys. Rev. Lett.*, vol. 107, 2011, Art. no. 253601.
[25] A. Shevchenko, M. Roussey, A. T. Friberg, and T. Setälä, "Ultrashort coherence times in partially polarized stationary optical beams measured by two-photon absorption," *Opt. Express*, vol. 23, pp. 31274–31285, 2015.
[26] K. Jan, H. Axel, and J. Andreas, "Second-order coherence properties of amplified spontaneous emission from a high-power tapered superluminescent diode," *Laser Phys. Lett.*, vol. 14, no. 8, 2017, Art. no. 086201.
[27] P. Janassek, S. Blumenstein, and W. Elsäer, "Recovering a hidden polarization by ghost polarimetry," *Opt. Lett.*, vol. 43, no. 4, pp. 883–886, 2018.
[28] P. Janassek, S. Blumenstein, and W. Elsäer, "Ghost spectroscopy with classical thermal light emitted by a superluminescent diode," *Phys. Rev. Appl.*, vol. 9, no. 2, 2018, Art. no. 021001.
[29] S. Hartmann, A. Molitor, and W. Elsäer, "Ultrabroadband ghost imaging exploiting optoelectronic amplified spontaneous emission and two-photon detection," *Opt. Lett.*, vol. 40, no. 24, pp. 5770–5773, 2015.
[30] S. Hartmann and W. Elsäer, "A novel semiconductor-based, fully incoherent amplified spontaneous emission light source for ghost imaging," *Sci. Rep.*, vol. 7, 2017, Art. no. 41866.
[31] F. Boitier, A. Godard, N. Dubreuil, P. Delaye, C. Fabre, and E. Rosencher, "Photon extrabunching in ultrabright twin beams measured by two-photon counting in a semiconductor," *Nature Commun.*, vol. 2, 2011, Art. no. 425.
[32] F. Boitier *et al.*, "Second order coherence of broadband down-converted light on ultrashort time scale determined by two photon absorption in semiconductor," *Opt. Express*, vol. 18, pp. 20401–20408, 2011.
[33] F. Boitier, A. Godard, N. Dubreuil, P. Delaye, C. Fabre, and E. Rosencher, "Two-photon counting interferometry," *Phys. Rev. A*, vol. 87, 2013, Art. no. 013844.

[34] B. Dayan, A. Pe'er, A. A. Friesem, and Y. Silberberg, "Two photon absorption and coherent control with broadband down-converted light," *Phys. Rev. Lett*, vol. 93, 2004, Art. no. 023005.
[35] B. Dayan, "Theory of two-photon interactions with broadband down-converted light and entangled photons," *Phys. Rev. A*, vol. 76, 2007, Art. no. 043813.
[36] S. Du, "Atomic-resonance-enhanced nonlinear optical frequency conversion with entangled photon pairs," *Phys. Rev. A*, vol. 83, 2011, Art. no. 033807.
[37] U. Fano, "Quantum theory of interference effects in the mixing of light from phase independent sources," *Amer. J. Phys.*, vol. 29, no. 8, pp. 539–545, 1961.
[38] R. P. Feynman, R. B. Leighton, and M. Sands, *The Feyman Lectures on Physics*, vol. 3. Beijing, China: Beijing World Publishing Corp, 2004.
[39] L. Mandel, "Quantum effects in one-photon and two-photon interference," *Rev. Mod. Phys.*, vol. 71, pp. S274–S282, 1999.
[40] R. Loudon, *The Quantum Theory of Light.* Oxford, U.K.: Oxford Univ. Press, 2000.
[41] G. Scarcelli, V. Berardi, and Y. Shih, "Quantum interference approach to two-photon correlation phenomena with chaotic light," *J. Mod. Opt.*, vol. 53, pp. 2279–2292, 2006.
[42] J. B. Liu and Y. Shih, "Nth-order coherence of thermal light," *Phys. Rev. A*, vol. 79, 2009, Art. no. 023819.
[43] L. B. Soldano and E. C. M. Pennings, "Optical multi-mode interference devices based on self-imaging: Principles and applications," *J. Lightw. Technol.*, vol. 13, no. 4, pp. 615–627, Apr. 1995.
[44] O. Frazão *et al.*, "All-fiber Mach-Zehnder curvature sensor based on multimode interference combined with a long-period grating," *Opt. Lett.*, vol. 32, pp. 3074–3076, 2007.
[45] A. Mehta, W. Mohammed, and E. G. Johnson, "Multimode interference-based fiber-optic displacement sensor," *IEEE Photon. Technol. Lett.*, vol. 15, no. 8, pp. 1129–1131, Aug. 2003.
[46] Q. Wang and G. Farrell, "All-fiber multimode interference based refractometer sensor: Proposal and design," *Opt. Lett.*, vol. 31, pp. 317–319, 2006.
[47] Y. Gong, T. Zhao, Y. J. Rao, and Y. Wu, "All-fiber curvature sensor based on multimode interference," *IEEE Photon. Technol. Lett.*, vol. 23, no. 11, pp. 679–681, Jun. 2011.
[48] E. Li, X. Wang, and C. Zhang, "Fiber-optic temperature sensor based on interference of selective higher-order modes," *Appl. Phys. Lett.*, vol. 89, 2006, Art. no. 091119.